Casson fluid behaviour on steady, 2-D Nanofluid flow past a stretching sheet in presence of Magnetic field, Melting heat transfer and Porous medium

P. Narender[*, 1] and T. Ramakrishna Goud [1]

[*] Department of Mathematics, M. V. S. R. College of Engineering, Nadergul, Hyderabad

[1] Department of Mathematics, University College of Science, Saifabad, Osmania University, Hyderabad,

[*]Corresponding author Email address: npalugula1978@gmail.com

Abstract:

Under the influence of melting heat transfer, porous media, thermophoresis, and Brownian motion phenomena, a viscous, incompressible, and electrically conducting nanofluid was seen to flow across a stretched sheet in this research's MHD boundary layer. During the course of this study, the boundary conditions for the momentum, temperature, and concentration boundary layers are converted into a set of nonlinear ordinary differential equations. These equations are then numerically solved by using the Runge-Kutta method and the shot approach. In order to demonstrate how the various flow parameters have an effect on velocity, temperature, and concentration, graphs are utilised. Additionally, tables containing various parameter values are provided in order to evaluate the numerical values of shear stress, heat transfer rate, and mass transfer rate. Inferences may then be drawn from these graphs, and the reliability of the data that was gathered can then be assessed.

Keywords: Casson fluid; Nanofluid; Melting heat transfer; Porous medium; Two-dimensional; MHD; Stretching sheet; R-K method;

DOI Number: 10.48047/NQ.2022.20.12.NQ773703 **NeuroQuantology2022;20(12): 3779-3799**

Nomenclature:

List of Symbols:

u, v: Velocity components in x and y axes respectively (m/s)

x, y: Cartesian coordinates measured along the stretching sheet (m)

f: Dimensionless stream function

f': Fluid velocity (m/s)

$\Pr$: Prandtl number

C: Fluid concentration $\left(mol/m^3\right)$

C_∞: Dimensional ambient volume fraction $\left(mol/m^3\right)$

T: Fluid temperature $\left(K\right)$

T_w: Temperature at the surface $\left(K\right)$

T_∞: Temperature of the fluid far away from the stretching sheet $\left(K\right)$

O: Origin

M: Magnetic field parameter

C_w: Dimensional concentration at the stretching surface $\left(mol/m^3\right)$

Nu_x: Rate of heat transfer coefficient (or)Nusselt number

Sh_x: Rate of mass transfer coefficient (or) Sherwood number

Cf: Skin-friction coefficient

C_f: Specific heat capacity at constant pressure

C_p: Specific heat capacity of nanoparticle material

B_o: Uniform magnetic field

Le: Lewis number

Nb: Brownian Motion parameter

Nt: Thermophoresis parameter

D_B: Brownian diffusion coefficient

D_T: Thermophoresis diffusion coefficient

a: Positive real number

q_w: Heat flux

q_m: Mass flux

n: Stretching sheet parameter

u_w: Reference velocity (m/s)

T_m: Melting surface temperature (K)

k^*: Permeability of the porous medium

K: Permeability parameter (m)

eISSN 1303-5150

C_s : Concentration susceptibility
Me : Melting heat transfer parameter
Re_x : Reynold's number
T_0 : Reference temperature (K)

Greek symbols:

τ : Cauchy Stress tensor
η : Dimensionless similarity variable
θ : Dimensionless temperature (K)
ϕ : Dimensionless nanofluid concentration $\left(mol/m^3\right)$
ν : Kinematic viscosity $\left(m^2/s\right)$
σ : Stefan-Boltzmann constant
ρ : Density
ρ_f : Density of the fluid
ρ_p : Density of nanoparticle material
β : Casson fluid material parameter
μ : Dynamic viscosity of the fluid
τ_w : Shear stress
β : Deborah number
κ : Thermal conductivity of the fluid
λ : Molecular mean free path
μ : Dynamic viscosity of the fluid
α^* : Shear rate
μ_B : Dynamic viscosity of the Casson fluid

Superscript:

$'$: Differentiation w.r.t η

Subscripts:

f : Fluid
w : Condition on the sheet
∞ : Ambient Conditions

1. Introduction:

Besides, the phenomenon of melting also plays a vital part in contemporary and sophisticated industrial processes. Melting heat transfer has wide industrial applications, such as casting, welding and magma solidification, permafrost melting and thawing of frozen ground, etc. Many research papers have been published on the effect of melting heat transfer. Roberts [1] was the first to establish the concept of heat transfer developed during the melting process of ice retained in a hot stream. Since then, numerous researchers have investigated the properties of the melting heat process, particularly because of its extensive use in the creation of semiconductor materials, crystal growth, optimal energy utilization, welding process, and magma solidification. Bachok et al. [2] evaluated the melting heat transfer from a heated, laminar stretching/shrinking flow near the stagnation point. The melting and radiative heat transfer of MHD nanofluid flow under the circumstances of velocity slip was simulated by Muhammad et al. [3]. Kakar et al. [4] studied melting heat transfer of a magnetized water-based hybrid nanofluid flow past over a stretching/shrinking wedge. Khashi'ie et al. [5] studied Melting heat transfer in hybrid nanofluid flow along a moving surface. Khan et al. [6] studied melting heat transportation in chemical reactive flow of third grade nanofluid with irreversibility analysis. Farroq et al. [7] studied melting heat transport of nanofluids due to stretching surface with Cattaneo-Christov thermal model using numerical solutions. Multiple solutions of melting heat transfer of MHD hybrid based nanofluid flow influenced by heat generation/absorption found by Nuwairan et al. [8]. Gorla et al. [9] presented a boundary layer analysis for a warm and laminar flow of nanofluid over a melting surface moving parallel to a uniform free stream. Chamkha et al. [10] analyzed the effect of transverse magnetic field on hydromagnetic, forced convection flow with heat and mass transfer of a nanofluid over a horizontal stretching plate under the influence of melting and heat generation or

eISSN 1303-5150

absorption. Ahmad and Pop [11] examined at the way the melting parameter affects the flow of mixed convective in a porous geometry. Ishak et al. [12] examined melting heat transfer in steady laminar flow over a moving surface. Hayat et al. [13] and Yacob et al. [14] extended the study of melting heat transfer to non-Newtonian fluid, and they examined melting heat transfer in the stagnation point flow of couple stress and micropolar fluid. Melting heat transfer of upper-convicted Maxwell fluid over stretching sheet was discussed by Hayat et al. [15].

In the current scenario, with improvements in modern technology, nanofluids play an essential role in various engineering and scientific applications due to the improvement in the interpretation of heat transfer mechanisms for sufficient cooling. Choi [16] is the first person to introduce the concept of nanofluid in 1995. The utilization of porous media, which including metal-based porous materials like copper foams in channels and temperature changes, is another alluring method for improving heat transmission in industrial systems. A solid matrix called a porous media has pores (voids) that are generally filled with liquid. Rigid, open-cell, and saturated porous media are those that have pores that are linked and totally filled with fluid to allow the fluid to pass through the voids. Recently, the method of employing both nanofluid and porous media has drawn a lot of attention and prompted in-depth research in this area. On the one hand, porous media increase the area of contact between a liquid and a solid surface, while on the other, nanoparticles distributed in nanofluid improve the heat conductivity effectively. It appears that utilizing both porous medium and nanofluid can significantly increase the efficiency of conventional thermal systems [17]. Mukhopadhyay [18] investigated the effect of radiative heat and the mixed convection on the boundary layer of viscous and incompressible fluid flow due to permeable stretching surface through a porous media. Shahid [19] delved the UCM fluid flow over a stretching sheet in a porous medium under the magnetic field effects. Zainal et al. [20] discussed both thermal radiation and magnetic field influences on hybrid nanofluid flow along a porous moving surface. Khan et al. [21] studied hybrid nanofluid flow induced by stretching sheet embedded in a porous medium with heat generation, thermal radiation and viscous dissipation. Thermal radiation and suction/injection impacts on time-dependent magnetic hybrid nanofluid flow towards a stretching surface were presented by Lund et al. [22]. Three-dimensional magnetite hybrid nanofluid flow towards a thermally radiated stretching surface under porous medium was numerically solved by Yusuf et al. [23]. Behseresht [24] discussed the effects of Brownian motion and thermophoresis forces on the natural convection heat transfer of nanofluids around a vertical cone placed in a saturated porous medium. The natural convective flow of nanofluids over a convectively heated vertical plate in a saturated Darcy porous medium is studied numerically by Ghalambaz et al. [25]. Mehryan et al. [26] have performed a computational investigation of a micropolar nanofluid flowing inside a cavity saturated by porous media considering the local thermal non-equilibrium model. Hayat et al. [27] used HAM to solve the problem of porous medium MHD stretched flow of nanofluid. Flow and heat transfer in magneto-nanofluid past an impulsively started porous flat plate in a rotating frame was studied by Das et al. [28]. Chamka et al. [29] discussed an unsteady heat and mass transfer from a stretching surface embedded in a porous medium with chemical reaction effects. Sugunamma [30] studied radiation and inclined magnetic field effects on an unsteady MHD free convection flow past an impulsively moving vertical plate in a porous medium.

Motivated by the above research work, the behaviour of Casson-Nanofluid flow over a non-linearly stretched sheet with effects of Melting heat transfer, Porous medium, Magnetic field, Thermophoresis, Brownian motion has not been studied as per the knowledge of the authors. Therefore, this occurrence is

eISSN 1303-5150

arrangement with in the present paper. The specific aims of this numerical study are as follows.

a) To build up a mathematical model for the effects of Melting heat transfer and Porous medium on the flow characteristics of an Nano-Casson fluid over a stretched sheet in presence of Magnetic field.
b) A numerical simulation of the flow-controlling model based on the shooting technique and employing the Runge-Kutta method.
c) Developing a MATHEMATICA code to find the numerical solutions.
d) Analyzing the effect of different physical properties on the velocity, temperature, and concentration profiles of the Casson-Nano fluid flow boundary layer.
e) Numerical values of the Skin-friction, heat transfer rate, and mass transfer coefficients are shown in tables as a function of changes in various technical factors.
f) Validation of the numerical approach by research into similar works.

In addition, the process of melting is very necessary for the complex industrial operations that are carried out nowadays. Casting, welding, solidifying magma, melting permafrost, and defrosting frozen ground are only few of the many industrial uses for melting heat transfer. Other applications include melting permafrost and defrosting frozen ground. A lot of research publications have been written on the subject of the impact that melting heat transfer may have. The theory of heat transmission proposed by Roberts [1] was shown to be correct when it was applied to the process of ice melting in a heated stream. Since that time, a significant number of researchers have investigated the characteristics of the melting heat process. This is mostly owing to the frequency with which it is used to make semiconductor materials, build crystals, efficiently utilise energy, weld, and solidify magma. The melting heat transfer in a heated, laminar stretching/shrinking flow was investigated by Bachok et al. [2], who conducted their research close to the stagnation point. Melting and radiative heat transfer in MHD nanofluid flow were modelled by Muhammad et al. [3] under conditions of velocity slip. The melting heat transfer of a magnetised water-based hybrid nanofluid flow was investigated by Kakar et al. [4] via the use of a stretching/shrinking wedge. The melting heat transfer in the flow of hybrid nanofluids across a moving surface was explored by Khashi'ie et al. [5]. Irreversibility research was used by Khan et al. [6] to examine third-grade nanofluid chemical reactive flow. The melting heat transfer of nanofluids formed by stretching surfaces was investigated by Farroq et al. [7] using numerical solutions to study the phenomenon. Using an MHD hybrid-based nanofluid flow that was controlled by heat generation/absorption, Nuwairan et al. [8] were able to show numerous processes of melting heat transfer. A boundary layer research was carried out by Gorla et al. [9] for a heated, laminar flow of nanofluid travelling perpendicular to a uniform free stream. The flow was observed as it passed over a melting surface. The researchers Chamkha et al. [10] analysed the influence of a transverse magnetic field on the effects of melting and heat generation or absorption on hydromagnetic, forced convection flow with heat and mass transfer of a nanofluid over a horizontal stretching plate. Specifically, they focused on how the magnetic field affected the flow of the nanofluid. The influence of the melting parameter on mixed convective flow in a porous structure was investigated by Ahmad and Pop [11]. Ishak and colleagues [12] investigated the transport of melting heat in a laminar flow over a moving surface in a continuous flow environment. The investigation of melting heat transfer was expanded to include non-Newtonian fluids by Hayat et al. [13] and Yacob et al. [14]. In addition to this, they investigated the transmission of melting heat at the stagnation point of pair stress and micropolar fluid. The researchers Hayat et al. [15] examined the

eISSN 1303-5150

transport of melting heat through a stretched sheet using an upper-conviction Maxwell fluid.

As a consequence of technological advancements, nanofluids play an important part in a variety of technical and scientific applications. This is possible as a direct result of a greater understanding of the mechanisms involved in heat transmission, which in turn makes adequate cooling possible. In 1995, Choi [16] was the first person to present the idea of a nanofluid to the scientific community. An additional exciting way for enhancing heat transfer in industrial systems is making use of porous media. Porous media based on metals, such as copper foams, are examples of metal-based porous materials that may be used in channels and temperature fluctuations. A porous media is a solid matrix that has voids that are often filled with liquid. Porous media may be either solid or porous. Because the pores in stiff, open-celled, saturated porous media are associated with one another and are completely saturated, it is possible for fluid to move through the voids. Recently, there has been a lot of focus placed on the use of nanofluid media in addition to porous media, which has inspired a lot of study into this particular field. The area of contact between a liquid and a solid surface is increased by a porous medium, while the heat conductivity of a nanofluid that contains nanoparticles scattered throughout it is substantially improved. It seems that the performance of traditional thermal systems may be greatly improved by using both porous medium and nanofluid at the same time [17]. Mukhopadhyay [18] looked into how radiative heat and mixed convection affected the boundary layer of a viscous and incompressible fluid flow that was produced by a permeable, stretched surface by means of a porous medium. He was interested in how these factors controlled the flow. When there was a magnetic field in the environment, Shahid [19] investigated the flow of UCM fluid through a stretched sheet in a porous media. In their study [20], Zainal and colleagues explored the effects of magnetic fields and heat radiation on the flow of a hybrid nanofluid over a moving porous surface. Specifically, they were interested in how these factors affect the flow of the nanofluid. Khan et al. [21] investigated hybrid nanofluid flow by stretching a sheet that was then immersed in a porous media. This included the production of heat, the radiation of thermal energy, and the dissipation of viscous energy. In their study [22], Lund and colleagues showed the effects of heat radiation and suction/injection on the time-dependent flow of magnetic nanofluids towards a stretched surface. Yusuf et al. [23] used a computer programme to tackle the problem of the flow of a three-dimensional magnetite hybrid nanofluid toward a thermally stretched surface that was surrounded by porous media. The effects of Brownian motion and thermophoresis forces on the natural convection heat transfer of nanofluids around a vertical cone put in a saturated porous media were examined by Behseresht [24]. The spontaneous convective flow of nanofluids is studied numerically by Ghalambaz et al. [25] who explore the flow of nanofluids across a convectively heated vertical plate in a saturated Darcy porous media. With the local thermal non-equilibrium model in mind, Mehryan et al. [26] conducted a numerical investigation of a micropolar nanofluid moving through a cavity that was filled with porous media. They did this while keeping in mind that the cavity was saturated. The issue of nanofluid MHD-extended flow in porous media was solved by Hayat et al. [27] using HAM as a solution. The researchers Das et al. [28] looked at the flow of magneto-nanofluid and how it transferred heat over a porous flat plate when they began their experiment abruptly. The erratic heat and mass transmission from a stretched surface that was immersed in a porous liquid was explored by Chamka et al. [29]. Chemical reaction effects were also taken into consideration. An unstable MHD free convection flow was investigated by Sugunamma [30] using a vertical plate that moved irregularly through a porous media. She looked at how radiation and an angled magnetic field affected the flow.

eISSN 1303-5150

To the best of the authors' knowledge, no one has looked at the impact of melting heat transfer, porous media, magnetic field, thermophoresis, or Brownian motion on the behaviour of Casson-Nanofluid flow over a non-linearly stretched sheet. The research that were referenced before served as the impetus for this lack of comprehension. As a direct result of this, the phenomenon in question is researched in the current study. These are the precise objectives of the numerical investigation being conducted.

a) To develop a mathematical model of the effect that porous media and melting heat transfer have on the flow properties of a nano-casson fluid across a stretched sheet when a magnetic field is present in the environment.
b) A shooting-based flow-controlling model represented by a numerical simulation that is based on the Runge-Kutta technique.
c) Creating the necessary code in MATHEMATICA to get the numerical solutions.
d) Investigating the ways in which various physical factors impact the Casson-Nano fluid flow boundary layer's profiles of velocity, temperature, and concentration.
e) Tables with quantitative data for changes in a variety of technical parameters are provided, including Skin-friction, Heat transfer rate, and Mass transfer coefficients.
f) Validation of the numerical technique by looking at publications that are pertinent to the topic.

2. Flow Governing Equations:

In this existing research work, the performance of Casson-nanofluid flow towards a non-linearly stretching sheet in presence of magnetic field, Melting heat transfer, Thermophoresis and Brownian motion effects is studied using numerical solutions. The flow geometry of this flow is shown in Fig. 1. For this research work, the following assumptions are made.

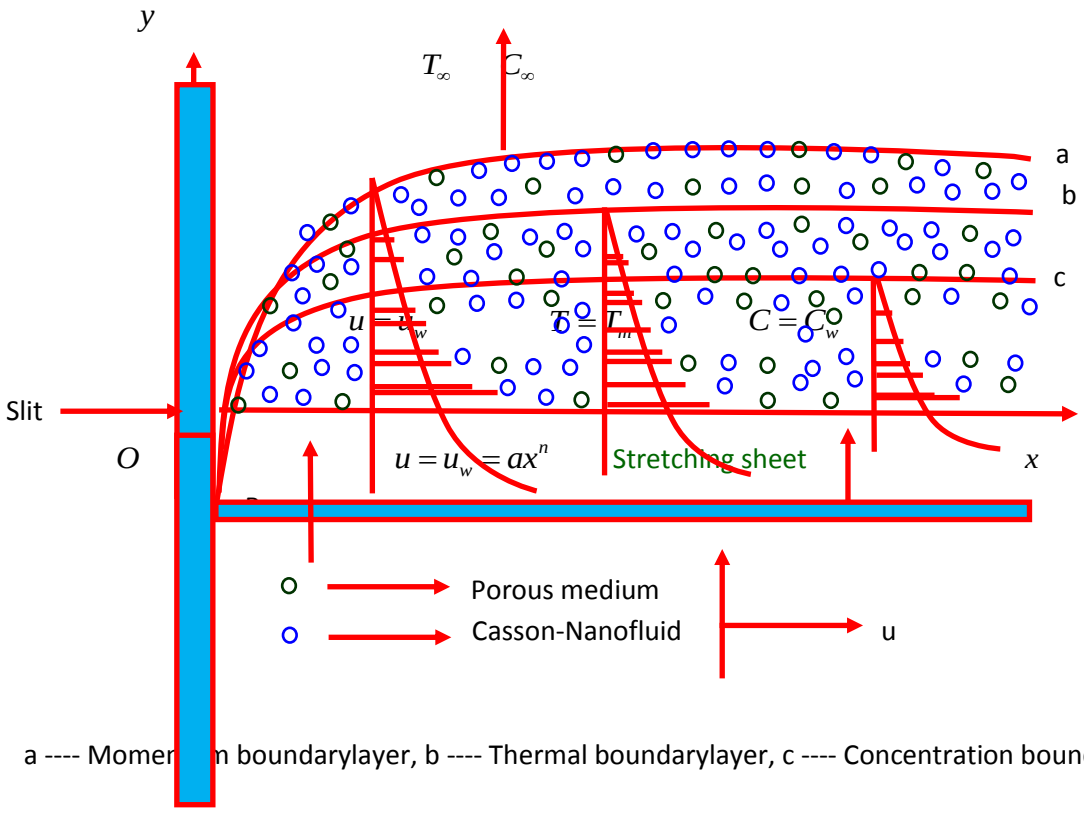

Fig. 1.: Geometry representation of the Casson-Nanofluid

eISSN 1303-5150

1. Let us consider the flow of a Casson-nanofluid through a stretching sheet that concurs with the plane $y = 0$ and is confined to the region $y > 0$.
2. The flow is constant, viscous, incompressible, and two-dimensional boundary layer flow.
3. It is produced as a result of non-linear stretching of the sheet, which is induced by the application of two equal and opposing pressures along the $x-$ axis at the same time.
4. When the origin is held constant, the sheet is then stretched with a velocity $u_w = ax^n$, where a denotes constant, n denotes nonlinear stretching parameter, and x is the coordinate along the stretching surface, which varies nonlinearly with distance from the slit.
5. Normally, a variable magnetic field B (x) will be provided to the surface of the sheet while the magnetic field induced is minimal and may be justified for MHD flow at the small magnetic Reynolds number.
6. The gradient of pressure and external forces are not taken into consideration.
7. The temperature and concentration of the stretching surface, T_w and C_w, are kept at constant values, and these values are considered to be higher than the temperature and concentration of the surrounding environment, T_∞ and C_∞, which are maintained at constant values.
8. The rheological equation for a non-Newtonian fluid is defined as, $\tau_1 = \tau_o + \mu_1 \alpha^*$ (1)
9. Eq. (1) can be expanded for Casson fluid as,

$$\tau_{ij} = \begin{cases} 2\left(\mu_B + \dfrac{p_y}{\sqrt{2\pi}}\right)e_{ij}, & \pi > \pi_c \\ 2\left(\mu_B + \dfrac{p_y}{\sqrt{2\pi_c}}\right)e_{ij}, & \pi < \pi_c \end{cases} \quad (2)$$

Where $\pi = e_{ij}e_{ji}$ with e_{ij} is the $(i, j)^{th}$ component of the fluid deformation rate and $p_y = \dfrac{\mu_B\sqrt{2\pi}}{\beta}$ is the yield stress of the Casson fluid.

Based on the above assumptions, the fundamental steady-state conservation of mass, momentum, thermal energy, and nanoparticles equations for Casson-Nanofluid can be written in Cartesian coordinates x and y as:

Continuity Equation:

$$\left(\frac{\partial u}{\partial x}\right) + \left(\frac{\partial v}{\partial y}\right) = 0 \quad (3)$$

Momentum Equation:

$$u\left(\frac{\partial u}{\partial x}\right) + v\left(\frac{\partial u}{\partial y}\right) = \nu\left(1 + \frac{1}{\beta}\right)\frac{\partial^2 u}{\partial y^2} - \left(\frac{\sigma B_o^2}{\rho_f}\right)u - \left(\frac{\mu}{k^*}\right)u \quad (4)$$

Equation of thermal energy:

$$u\left(\frac{\partial T}{\partial x}\right) + v\left(\frac{\partial T}{\partial y}\right) = \frac{\kappa}{(\rho C)_f}\left(\frac{\partial^2 T}{\partial y^2}\right) + \left[\frac{(\rho C)_p}{(\rho C)_f}\right]\left\{D_B\left(\frac{\partial C}{\partial y}\right)\left(\frac{\partial T}{\partial y}\right) + \left(\frac{D_T}{T_\infty}\right)\left(\frac{\partial T}{\partial y}\right)^2\right\} \quad (5)$$

Equation of species concentration:

$$u\left(\frac{\partial C}{\partial x}\right) + v\left(\frac{\partial C}{\partial y}\right) = D_B\left(\frac{\partial^2 C}{\partial y^2}\right) + \left(\frac{D_T}{T_\infty}\right)\left(\frac{\partial^2 T}{\partial y^2}\right) \quad (6)$$

eISSN 1303-5150

Subject to the boundary conditions for Casson-nano fluid flow with are

$$\left.\begin{array}{l} u = u_w(x),\ v = 0,\ T = T_m,\ \kappa\left(\dfrac{\partial T}{\partial y}\right)_{y=0} = \rho\left(\lambda + C_s\left(T_m - T_o\right)\right)v(x,\ 0),\ C = C_w\ at\ \ y = 0 \\ u \to 0,\ v \to 0,\ T \to T_\infty,\ C \to C_\infty\ \ as\ \ y \to \infty \end{array}\right\}, \quad (7)$$

The following similarity variables are introduced for solving governing equations (4)-(6) as

$$\left.\begin{array}{l} \eta = y\left(\sqrt{\dfrac{a(n+1)}{2\nu}}\right)x^{\frac{n-1}{2}},\ u = ax^n f'(\eta),\ v = -\left(\sqrt{\dfrac{a\nu(n+1)}{2}}\right)x^{\frac{n-1}{2}}\left(f(\eta) + \left(\dfrac{n-1}{n+1}\right)\eta f'(\eta)\right), \\ \theta(\eta) = \dfrac{T - T_\infty}{T_m - T_\infty},\ \phi(\eta) = \dfrac{C - C_\infty}{C_w - C_\infty} \end{array}\right\} \quad (8)$$

Using Eq. (8), the fundamental Eqs. (4) to (6) become

$$\left(1 + \frac{1}{\beta}\right)f''' + ff'' - \left(\frac{2n}{n+1}\right)f'^2 - (M + K)f' = 0 \quad (9)$$

$$\theta'' + \Pr f\theta' + \Pr Nb\theta'\phi' + \Pr Nt\theta'^2 = 0 \quad (10)$$

$$2Nb\phi'' + NbLef\phi' + 2Nt\theta'' = 0 \quad (11)$$

and the corresponding boundary conditions (7) become

$$\left.\begin{array}{l} f'(0) = 1,\ \theta(0) = 0,\ Me\theta'(0) + \Pr f(0) = 0,\ \phi(0) = 1 \\ f'(\infty) \to 0,\ \theta(\infty) \to 0,\ \phi(\infty) \to 0 \end{array}\right\}, \quad (12)$$

where the involved physical parameters are defined as

$$\left.\begin{array}{l} \Pr = \dfrac{\nu}{\alpha},\ M = \dfrac{\sigma B_o^2 x}{\rho_f a},\ Le = \dfrac{\nu}{D_B},\ Nb = \dfrac{(\rho C)_p D_B(C_w - C_\infty)}{(\rho C)_f \nu},\ Nt = \dfrac{(\rho C)_p D_T(T_m - T_\infty)}{(\rho C)_f \nu T_\infty}, \\ Me = \dfrac{C_f(-T_m + T_\infty)}{\lambda + C_s(-T_m + T_\infty)},\ K = \dfrac{\nu}{ak^*} \end{array}\right\} \quad (13)$$

The parameters of engineering interest in heat and mass transport problems are the Skin-friction coefficient (Cf), local Nusselt number (Nu_x) and the Sherwood number (Sh_x) are defined as

$$Cf = \left(1 + \frac{1}{\beta}\right)\frac{\tau_w}{\rho_f U^2} \Rightarrow \left(\sqrt{\mathrm{Re}_x}\right)Cf = \left(1 + \frac{1}{\beta}\right)f''(0) \quad (14)$$

$$Nu_x = \frac{xq_w}{\kappa(T_m - T_\infty)} \text{ where } q_w = -\kappa(T_m - T_\infty)x^{\frac{n-1}{2}}\left(\sqrt{\frac{a(n+1)}{2\nu}}\right)\theta'(0)$$

$$\Rightarrow Nu_x = -x^{\frac{n+1}{2}}\left(\sqrt{\frac{a(n+1)}{2\nu}}\right)\theta'(0) \quad (15)$$

$$Sh_x = \frac{xq_m}{D_B(C_w - C_\infty)} \text{ where } q_m = -D_B(C_w - C_\infty)x^{\frac{n-1}{2}}\left(\sqrt{\frac{a(n+1)}{2\nu}}\right)\phi'(0)$$

$$\Rightarrow Sh_x = -x^{\frac{n+1}{2}}\left(\sqrt{\frac{a(n+1)}{2\nu}}\right)\phi'(0) \quad (16)$$

3. Numerical Solutions by Runge-Kutta Method with Shooting Technique:

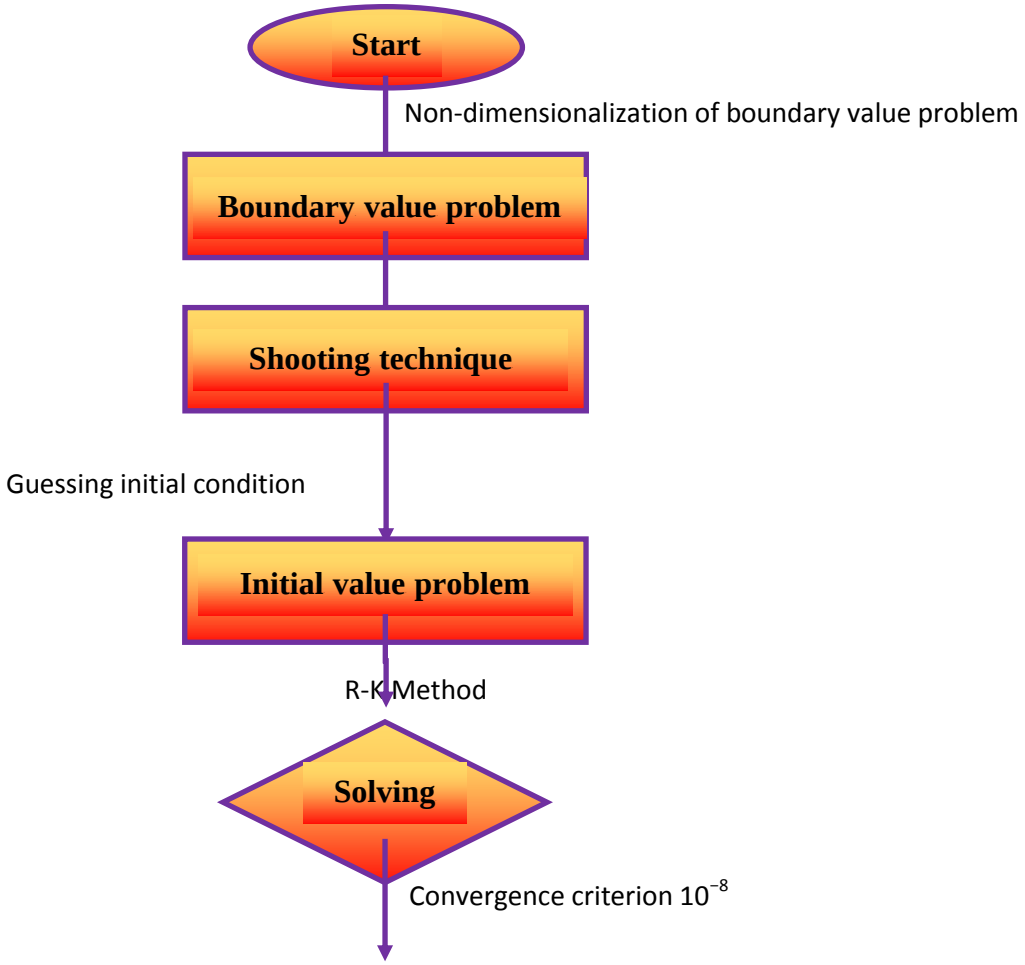

Fig. 3.: Flow diagram of the numerical procedure

In order to solve the system of ordinary differential equations (9)-(11) with their corresponding initial and boundary conditions (12) numerically, the domain [0, ∞) has been substituted by the bounded domain $[0,\ \eta_\infty]$ where η_∞ is a suitable finite real number that should be chosen in such a way that the solution satisfies the domain. Also (9)-(11) form a highly nonlinear coupled initial boundary value problem of third and second order ODEs. For this reason, (9)-(11) have been reduced to a system of seven initial problems of the first order of seven unknowns from the following the supposition in

$$f = y_1,\ f' = y_2,\ f'' = y_3,\ f''' = y_4,\ \theta = y_5,\ \theta' = y_6,\ \phi = y_7,\ \phi' = y_8\} \quad (17)$$

Thus we develop the most effective numerical technique in line with the fourth order Runge-Kutta shooting technique. The symbolic software MATHEMATICA is used to obtain the numerical solution. To solve this system, we require seven initial conditions whereas we have only four initial conditions for $f(0),\ f'(0),$ $\theta(0)$ and $\phi(0)$, while the other three $f''(0), \theta'(0)$ and $\phi'(0)$ were not given; hence, we employ numerical shooting technique where these three initial conditions are guessed to produce the required three ending boundary conditions. During the mathematical simulation, the step size is to be $\Delta\eta$ = 0.001 in order to acquire results. The criterion of convergence is 10^{-8}. The subsequent procedure is visualized through Fig. 2.

eISSN 1303-5150

4. Program Code Validation:

For checking of program code validation, the present the results of Nusselt and Sherwood numbers are compared with the published results of Rana and Bhargava [31] in tables 1, 2, 3 and 4 respectively for various values of Pr, n, Le, Nb and Nt at $\beta \to \infty,\ M = Me = K = 0$. From these tables it is observed that, there is an excellent correlation has been achieved with the earlier results of Rana and Bhargava [31].

Table-1.: Comparison of present rate of heat transfer coefficient (Nusselt number) results with published rate of heat transfer (Nusselt number) results of Rana and Bhargava [31] for various values of n, Nt and Nb when $\beta \to \infty,\ M = Me = K = 0$

n	Nt	Present $-\theta'(0)$ results			Published $-\theta'(0)$ results of Rana and Bhargava [31]		
		Nb = 0.5	Nb = 1.0	Nb = 2.5	Nb = 0.5	Nb = 1.0	Nb = 2.5
0.2	0.1	0.50858943	0.26969834	0.02935694	0.5160	0.2775	0.0303
	0.3	0.44867982	0.23867896	0.02595492	0.4533	0.2427	0.0265
	0.5	0.38679198	0.20967391	0.02286793	0.3999	0.2135	0.0234
3.0	0.1	0.47855012	0.41988026	0.36952417	0.4864	0.4282	0.3786
	0.3	0.41788523	0.21988751	0.02499612	0.4282	0.2293	0.0251
	0.5	0.36899529	0.19985127	0.02188632	0.3786	0.2020	0.0221
10.0	0.1	0.46877123	0.24788034	0.01988699	0.4799	0.2581	0.0283
	0.3	0.41899930	0.21998647	0.02388797	0.4227	0.2263	0.0247
	0.5	0.36887412	0.19654329	0.01988734	0.3739	0.1996	0.0214

Table-2.: Comparison of present rate of mass transfer coefficient (Sherwood number) results with published rate of mass transfer (Sherwood number) results of Rana and Bhargava [31] for various values of n, Nt and Nb when $\beta \to \infty,\ M = Me = K = 0$

n	Nt	Present $-\phi'(0)$ results			Published $-\phi'(0)$ results of Rana and Bhargava [31]		
		Nb = 0.5	Nb = 1.0	Nb = 2.5	Nb = 0.5	Nb = 1.0	Nb = 2.5
0.2	0.1	0.89777321	0.93844326	0.93996102	0.9012	0.9413	0.9493
	0.3	0.82966307	0.92988037	0.94830678	0.8395	0.9394	0.9571
	0.5	0.79802145	0.93980123	0.95703649	0.8048	0.9429	0.9642
3.0	0.1	0.83861278	0.79321048	0.72993102	0.8445	0.7785	0.7379
	0.3	0.76922314	0.86733099	0.88751698	0.7785	0.8792	0.8997
	0.5	0.72981035	0.86976013	0.89766352	0.7379	0.8793	0.9056
10.0	0.1	0.82560374	0.86933715	0.87952014	0.8323	0.8722	0.8812
	0.3	0.75996312	0.85961237	0.87992135	0.7654	0.8662	0.8873
	0.5	0.71980364	0.85900674	0.88693475	0.7238	0.8656	0.8930

Table-3.: Comparison of present rate of heat transfer coefficient (Nusselt number) results with published rate of heat transfer (Nusselt number) results of Rana and Bhargava [31] for various values of Pr, n and Le when $\beta \to \infty,\ M = Me = K = 0$

Pr	n	Present $-\theta'(0)$ results			Published $-\theta'(0)$ results of Rana and Bhargava [31]		
		Le = 2.0	Le = 10.0	Le = 25.0	Le = 2.0	Le = 10.0	Le = 25.0
0.7	0.2	0.31882013	0.29633052	0.28752154	0.3299	0.3042	0.2982
	0.5	0.31986247	0.28795532	0.28996321	0.3216	0.2965	0.2906
	3.0	0.29633152	0.27963263	0.26558263	0.3053	0.2812	0.2757
2.0	0.2	0.38779201	0.27966636	0.24898302	0.3999	0.2835	0.2569
	0.5	0.38962895	0.26855413	0.24785325	0.3930	0.2778	0.2517
	3.0	0.36687521	0.25804132	0.23988632	0.3786	0.2661	0.2410
7.0	0.2	0.21899752	0.04966735	0.03396798	0.2248	0.0547	0.0345
	0.5	0.21887879	0.04673121	0.03186629	0.2261	0.0546	0.0328
	3.0	0.21799326	0.04869677	0.03089667	0.2288	0.0537	0.0319

Table-4.: Comparison of present rate of mass transfer coefficient (Sherwood number) results with published rate of mass transfer (Sherwood number) results of Rana and Bhargava [31] for various values of Pr, n and Le when $\beta \to \infty,\ M = Me = K = 0$

Pr	n	Present $-\phi'(0)$ results			Published $-\phi'(0)$ results of Rana and Bhargava [31]		
		Le = 2.0	Le = 10.0	Le = 25.0	Le = 2.0	Le = 10.0	Le = 25.0
0.7	0.2	0.80955878	2.30966451	3.81755234	0.8132	2.3198	3.8262
	0.5	0.78533145	2.28993677	3.79532478	0.7965	2.2959	3.8005
	3.0	0.75966834	2.23988634	3.73988436	0.7630	2.2464	3.7471
2.0	0.2	0.79866569	2.41899630	3.94865794	0.8048	2.4207	3.9547
	0.5	0.77966541	2.26998766	3.91866589	0.7826	2.2778	3.9245
	3.0	0.72966348	2.32996472	3.85973420	0.7379	2.3324	3.8616
7.0	0.2	1.00108662	2.61876524	4.11986324	1.0114	2.6202	4.1223
	0.5	0.97866548	2.57635087	4.08937546	0.9808	2.5871	4.0909
	3.0	0.90866423	2.50899642	4.01887655	0.9185	2.5194	4.0224

5. Results and Discussion:

In the previous section, the system of equations (9)-(11) is numerically solved by asset of shooting technique with fourth order R-K scheme. In this section, the impacts of different strong parameters namely, Magnetic field parameter (M), Prandtl number (Pr), Casson fluid parameter (β), Stretching sheet parameter (n), Permeability parameter (K), Brownian motion parameter (Nb), Thermophoresis parameter (Nt), Melting heat transfer parameter (Me), and Lewis parameter (Le) on the flow profiles namely velocity profiles,

eISSN 1303-5150

temperature profiles and concentration profiles are shown in Fig. 3, Fig. 4, Fig. 5, Fig. 6, Fig. 7, Fig. 8, Fig. 9, Fig. 10, Fig. 11, Fig. 12, Fig. 13. Also, the numerical values of Skin-friction, Nusselt and Sherwood number coefficients for the different values of the above said parameters are offered in Table-5, Table-6 and Table-7 respectively.

- ➔ The strength of the magnetic field parameter (M) in Fig. 3 has an impact on the velocity profiles. It has been observed that the magnetic parameter has an inverse relationship with the velocity parameter. A force known as the Lorentz force is generated when one increases the value of the magnetic parameter. In contrast to the fluid particle's mobility, the production of this force results in the generation of a resistive force. As a consequence, the velocity of the vehicle drops.
- ➔ Fig. 4 illustrates the effect of the Permeability parameter (K) on the velocity distribution. As the Permeability (porosity) parameter K is increased, the velocity profile decreases, as demonstrated in this picture. The porous layer is amplified as K increases, diminishing the thickness of the momentum boundary layer.
- ➔ The effect of Casson parameter (β) on velocity profiles is shown in Fig. 5. It is examined that with growth in Casson parameter there is decline in velocity profile. It can be explained as surface near the velocity of the sheet exhibits the increasing behaviour due to the existence of slip boundary conditions. So increase in Casson parameter causes to decrease in yield stress which allows less resistance to the motion of fluid elements.
- ➔ Fig. 6 depicts the variations of velocity profiles for different values of stretching parameter (n) values. The conclusion that can be taken from this result is that the velocity profiles get flatter as the quantity of n rises. In other words, when the non-linear stretching parameter n is increased, the thickness of the momentum barrier layer will decrease as well.
- ➔ Illustration of the influence of Prandtl number (Pr) on temperature profiles is shown in Fig. 7. Increased Prandtl number Pr measurements over a certain threshold indicate that the temperature has decreased. When the thermal diffusivity and Prandtl number are inverted, a cooling effect is seen.
- ➔ The effect of the Brownian motion parameter (Nb) on temperature and concentration profiles is shown in Figs. 8 and 9. The temperature profile settled at higher values by an increase in the Brownian motion parameter. Brownian motion is the random motion due to the collisions between nanoparticles and base fluid. More is the Brownian motion parameter; more is the collision. Due to collision between particles, the internal kinetic energy of the fluid increases. There is a reverse relationship between the Brownian motion parameter and concentration profile. More is the Brownian motion parameter; less is the number of nanoparticles in the base fluid.
- ➔ Figs. 10 and 11 reveal the impact of thermophoresis parameter (Nt) on temperature and concentration profiles. Both temperature and concentration profiles increase for higher values of Nt. Thermophoresis is the transport force that occurs due to the temperature gradient between layers of the fluid. More Thermophoresis parameter means that the temperature difference between the layer increases, so the heat transformation rate also increases. By increasing the nanoparticles, the concentration of the fluid increases. More is the nanoparticles more is the heat transformation between the layers, so Nt increases both temperature profiles as well as concentration profiles.

eISSN 1303-5150

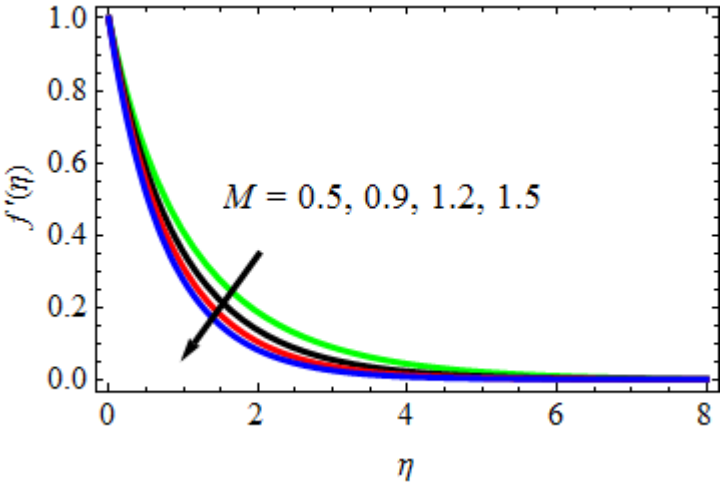

Fig. 3. M influence on velocity profiles $f'(\eta)$

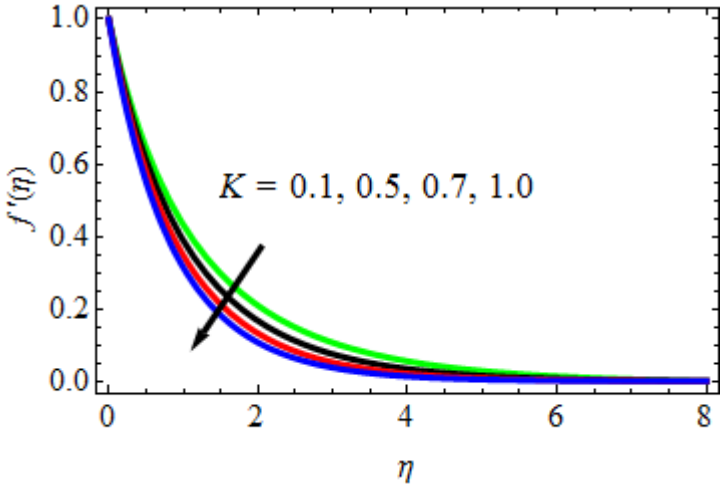

Fig. 4. K influence on velocity profiles $f'(\eta)$

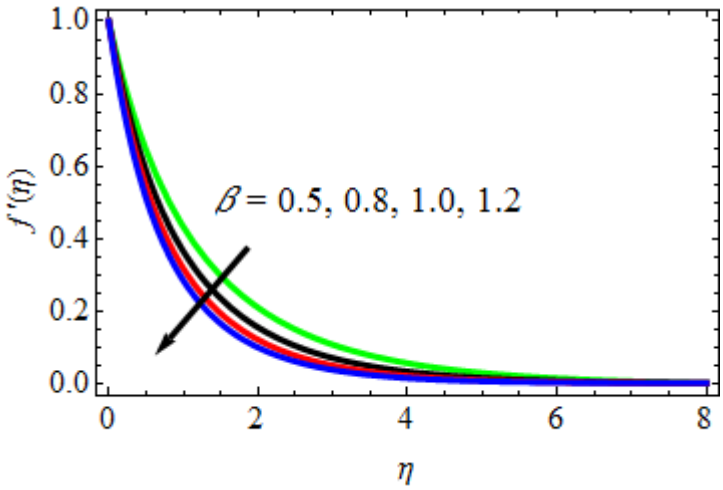

Fig. 5. β influence on velocity profiles $f'(\eta)$

eISSN 1303-5150

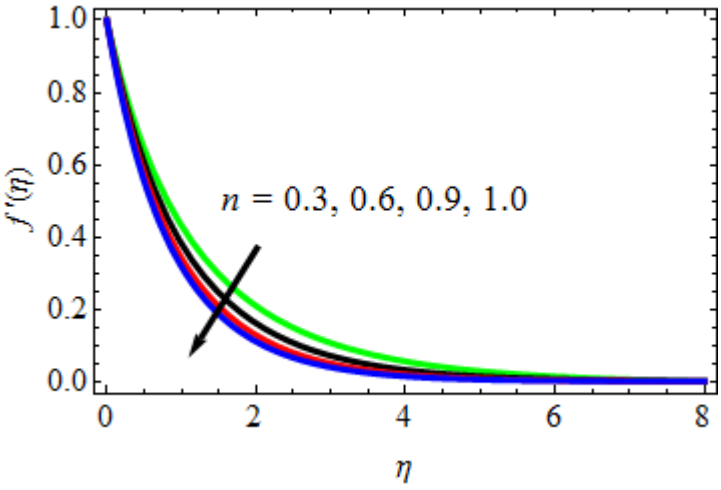

Fig. 6. n influence on velocity profiles $f'(\eta)$

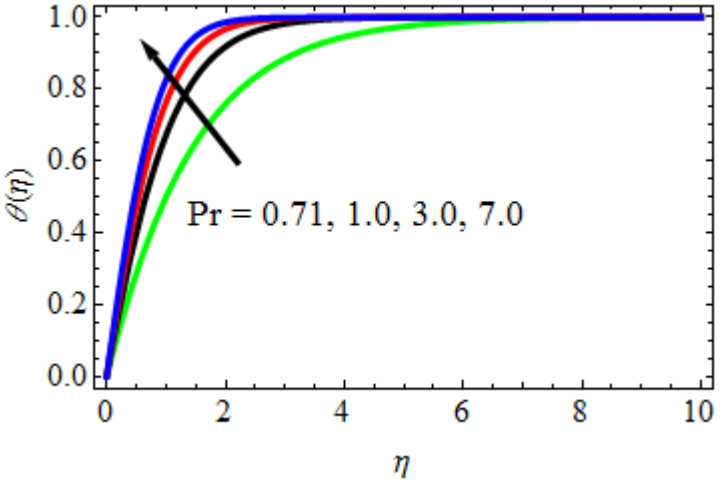

Fig. 7. Pr influence on temperature profiles $\theta(\eta)$

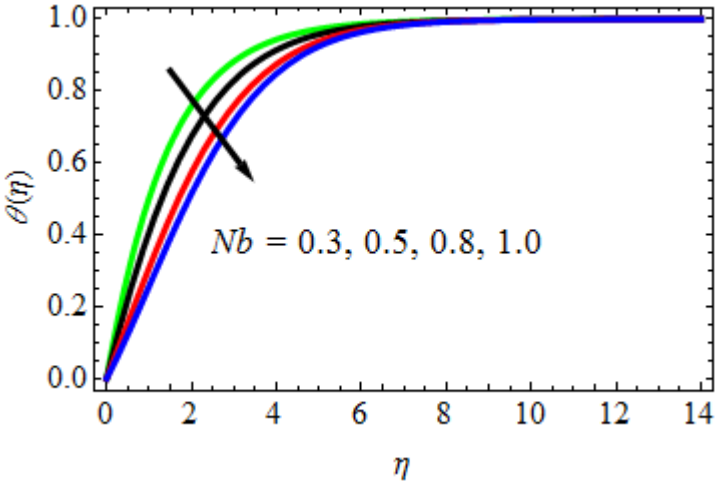

Fig. 8. Nb influence on temperature profiles $\theta(\eta)$

eISSN 1303-5150

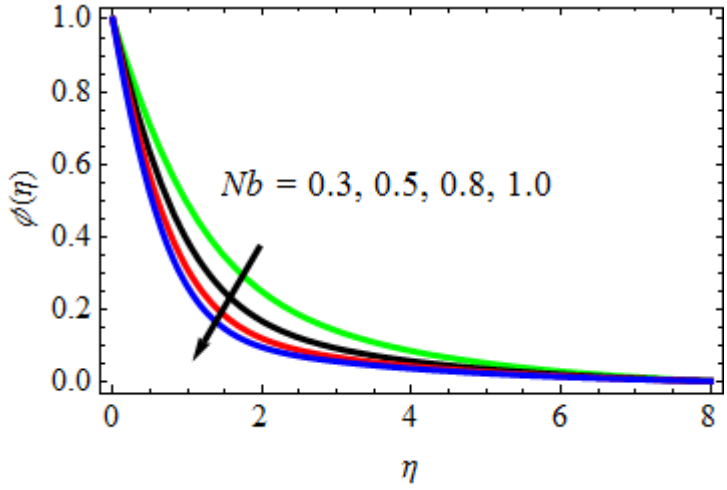

Fig. 9. Nb influence on concentration profiles $\phi(\eta)$

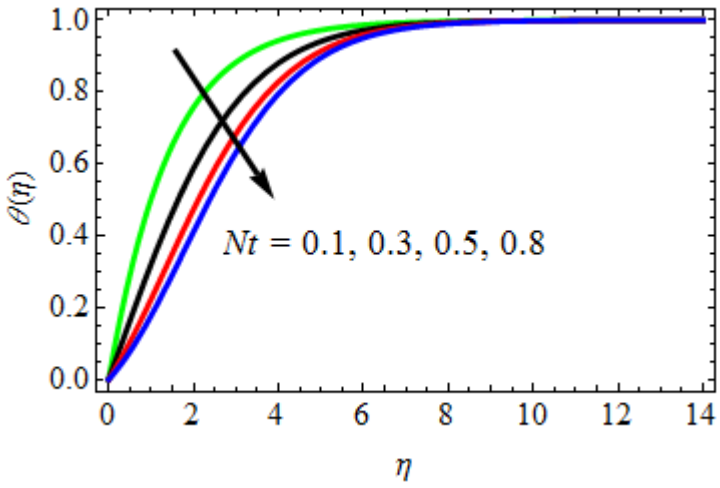

Fig. 10. Nt influence on temperature profiles $\theta(\eta)$

eISSN 1303-5150

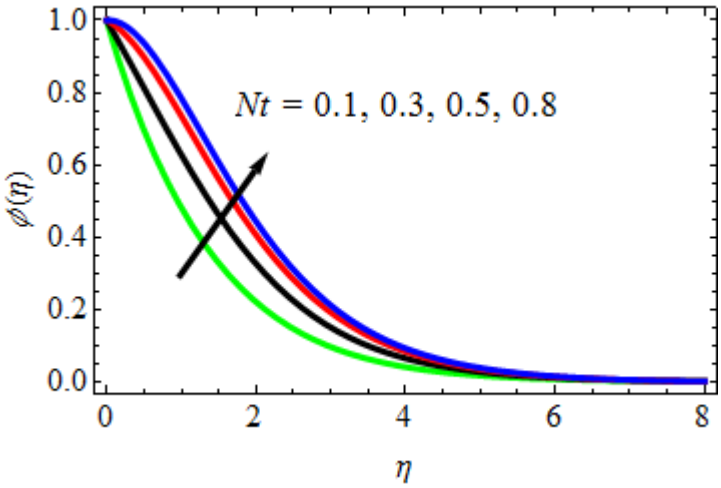

Fig. 11. Nt influence on concentration profiles $\phi(\eta)$

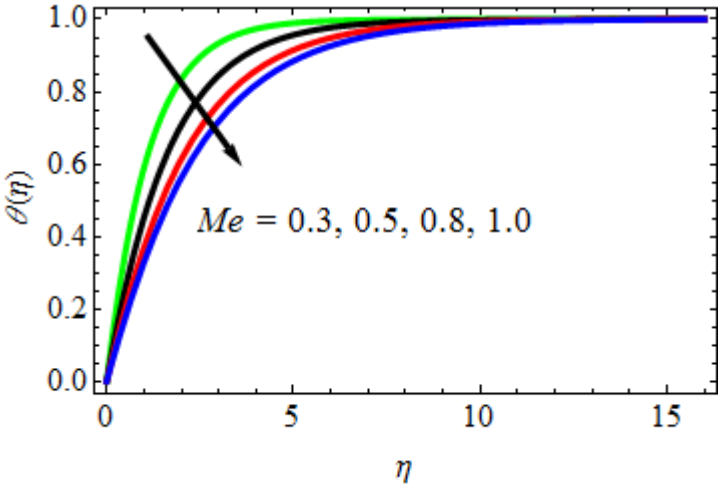

Fig. 12. Me influence on temperature profiles $\theta(\eta)$

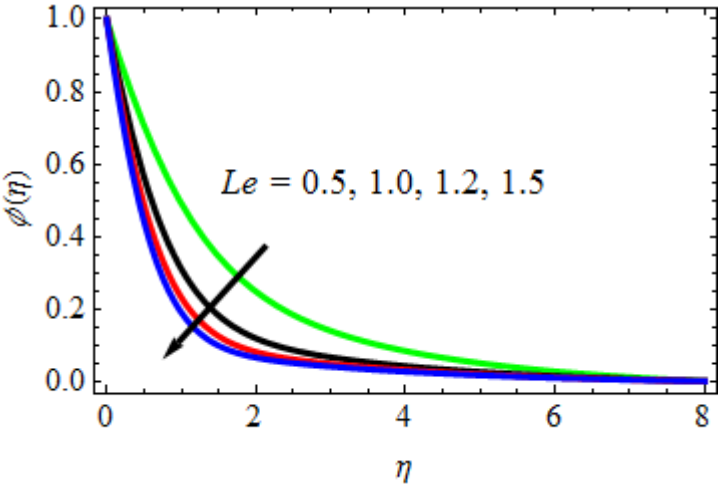

Fig. 13. Le influence on concentration profiles $\phi(\eta)$

eISSN 1303-5150

- The influence of melting parameter Me on temperature graph is plotted in Fig. 12. As the values of Me increases, the graph asymptotically approaches to 1.0 and the thermal boundary layer thickness increases. Increasing the melting parameter Me causes an increase in thermal diffusivity of a fluid. As a result, a heat transfer rate increases. Besides, the influence of melting parameter Me nanofluid is less than any ordinary fluids. Physically, increasing the melting parameter Me causes higher acceleration to the fluid flow which, in turn, increases its motion and causes decrease in the temperature profiles.

- Fig. 13 depicts the correlation between concentration and the nanofluid Lewis number (Le). This is a Lewis number, and the Lewis number describes the ratio of the heat and mass diffusivity for a dimensionless nanofluid. Increasing the value of Le results in a substantial reduction in the nanoparticle volume percentage.

Table-5.: Skin-friction coefficient (Cf) results for variations of M, Pr, β, n, K, Nb, Nt, Me and Le

M	K	n	β	Pr	Nb	Nt	Le	Me	Skin-friction coefficient
0.5	0.1	0.3	0.5	0.71	0.3	0.1	0.5	0.3	1.852002156484306598
0.9									1.725564102598745636
1.2									1.649804391904393474
1.5									1.627438919589168533
	0.5								1.826783468761818346
	0.7								1.784718734875837457
	1.0								1.755678018764837468
		0.6							1.805758787034687549
		0.9							1.774471709363470994
		1.0							1.756589273434870837
			0.8						1.814890137643874066
			1.0						1.796748317176309873
			1.2						1.774731909387996519
				1.0					1.796758719374985694
				3.0					1.765715756103473173
				7.0					1.747498313461743701
					0.5				1.885801764359594839
					0.8				1.916782983473347138
					1.0				1.936789367819868879
						0.3			1.906784717348445664
						0.5			1.946781957649014688
						0.8			1.966785798189346785
							1.0		1.825470173476347340
							1.2		1.806781739098483929
							1.5		1.786789319396749302
								0.5	1.885791389276178346
								0.8	1.916771786378643103
								1.0	1.938738187337448937

Table-6.: Nusselt number coefficient results for different values of Pr, Nb, Nt and Me

Pr	Nb	Nt	Me	Nusselt number coefficient
0.71	0.3	0.1	0.3	0.788970171387475347
1.00				0.708988184735684693
3.00				0.685687145841383837
7.00				0.664649177643873496
	0.5			0.757850734587178378
	0.8			0.726710736473743798
	1.0			0.706789037187398938
		0.3		0.810987091346707353
		0.5		0.835391013873013610
		0.8		0.856738187395681378
			0.5	0.825787108733737483
			0.8	0.855810983643773939
			1.0	0.889471936587468733

Table-7.: Sherwood number coefficient results for various values of Nb, Nt and Le

Nb	Nt	Le	Sherwood number coefficient
0.3	0.1	0.5	0.585678734858770834
0.5			0.556798398374187483
0.8			0.525613659638793707
1.0			0.505857901987563936
	0.3		0.645671892536198765
	0.5		0.665691348274235711
	0.8		0.695671374673856766
		1.0	0.545671873460873478
		1.2	0.516771730173739360
		1.5	0.490968710346937379

➔ Table-5 shows the numerical values of Skin-friction coefficient (Cf) for variations in values of the engineering parameters such as, Magnetic field parameter (M), Prandtl number (Pr), Casson fluid parameter (β), Stretching sheet parameter (n), Permeability parameter (K), Brownian motion parameter (Nb), Thermophoresis parameter (Nt), Melting heat transfer parameter (Me), and Lewis parameter (Le). From this table, it is observed that the Skin-friction coefficient is increasing with rising values of Brownian motion parameter (Nb), Thermophoresis parameter (Nt), Melting heat transfer parameter (Me), while it is decreasing with increasing values of Magnetic field parameter (M), Prandtl number (Pr), Casson fluid parameter (β), Stretching sheet parameter (n), Permeability parameter (K), and Lewis parameter (Le).

eISSN 1303-5150

- ➔ The numerical values of rate of heat transfer coefficient in terms of Nusselt number are displayed in Table-6 for different values of Prandtl number (Pr), Brownian motion parameter (Nb), Thermophoresis parameter (Nt), Melting heat transfer parameter (Me). The rate of heat transfer coefficient is gradually rising with increasing values of Brownian motion parameter (Nb), Thermophoresis parameter (Nt), Melting heat transfer parameter (Me), while the reverse effect is observed in increasing values of Prandtl number (Pr).
- ➔ The effects of Brownian motion parameter (Nb), Thermophoresis parameter (Nt) and Lewis number (Le) on the rate of mass transfer coefficient or in terms Sherwood number coefficient are discussed in Table-7. From this table, it is observed that the rate of mass transfer coefficient is increasing with increasing values of Thermophoresis parameter (Nt) and decreasing with increasing values of Brownian motion parameter (Nb) and Lewis number (Le).

6. Conclusions:

The objective of this research is to examine the steady, incompressible, two-dimensional, viscous, electrically conducting flow of a non-Newtonian Casson-nanofluid over a stretching surface with Melting heat transfer, Magnetic field, Porous medium, Thermophoresis and Brownian motion effects. The present problem is solved with the help of numerical technique called R-K method along with Shooting technique. The impacts of embedded parameters like magnetic parameter, Magnetic field parameter (M), Prandtl number (Pr), Casson fluid parameter (β), Stretching sheet parameter (n), Permeability parameter (K), Brownian motion parameter (Nb), Thermophoresis parameter (Nt), Melting heat transfer parameter (Me), and Lewis parameter (Le) on the flow profiles are displayed with the help of figures. The list of concluding remarks are:

- ✓ Velocity profile rises with the increment in the Thermophoresis (Nt), Brownian motion (Nb) and Melting heat transfer (Me).
- ✓ The velocity distribution is decreasing function of Magnetic field parameter (M), Casson fluid material parameter (γ) and Stretching sheet parameter (n).
- ✓ Temperature profiles are decrease for increasing of Prandtl number (Pr), while it increases for increasing of Thermophoresis (Nt), Melting heat transfer (Me) and Brownian motion (Nb),.
- ✓ The concentration diminishes with increase in Brownian motion (Nb), Lewis number (Le) and reverse effect is observed in case of Thermophoresis (Nt).
- ✓ In order to ensure validity, the findings are also compared with previously published results, which are found to be in fairly good agreement.
- ✓ These results from this investigation will help in promoting quality nanotechnology and industrial products. It will as well assist in the appropriate combination and utilization of non-Newtonian fluids for the chemical engineering, thermal sciences, biotechnology and others.

References:

1. L. Roberts, On the melting of a semi-infinite body of ice placed in a hot stream of air, J. Fluid Mech., 4 (5) (1958), pp. 505-528, 10.1017/S002211205800063X.
2. N. Bachok, A. Ishak, I. Pop, Melting heat transfer in boundary layer stagnation-point flow towards a stretching/shrinking sheet, Phys. Lett. A., 374 (40) (2010), pp. 4075-4079.
3. T. Muhammad, H. Waqas, U. Farooq, M. S. Alqarni, Numerical simulation for melting heat transport in nanofluids due to quadratic stretching plate with nonlinear thermal radiation, Case Stud. Therm. Eng., 27 (2021), p. 101300, 10.1016/j.csite.2021.101300.

4. N. Kakar, A. Khalid, A. S. Al-Johani, N. Alshammari, I. Khan, Melting heat transfer of a magnetized water-based hybrid nanofluid flow past over a stretching/shrinking wedge, Case Stud. Therm. Eng., 30 (2022), p. 101674, 10.1016/j.csite.2021.101674.
5. N. S. Khashi'ie, N. Md. Arifin, I. Pop, R. Nazar, Melting heat transfer in hybrid nanofluid flow along a moving surface, J. Therm. Anal. Calorim., 147 (1) (2022), pp. 567-578.
6. S. A. Khan, M. I. Khan, F. Alzahrani, Melting heat transportation in chemical reactive flow of third grade nanofluid with irreversibility analysis, Int. Commun. Heat Mass Transf., 129 (2021), p. 105696.
7. U. Farooq, H. Waqas, M. Imran, A. Albakri, T. Muhammad, Numerical investigation for melting heat transport of nanofluids due to stretching surface with Cattaneo-Christov thermal model, Alex. Eng. J., 61 (9) (2022), pp. 6635-6644, 10.1016/j.aej.2021.12.020.
8. M. Al Nuwairan, A. Hafeez, A. Khalid, A. Aldhafeeri, Multiple solutions of melting heat transfer of MHD hybrid based nanofluid flow influenced by heat generation/absorption, Case Stud. Therm. Eng., 35 (2022), p. 101988, 10.1016/j.csite.2022.101988
9. R. S. R. Gorla, A. Chamkha, A. Aloraier, Melting heat transfer in a nanofluid flow past a permeable continuous moving surface, J. Nav. Arch. Mar. Eng, 2 (2011), pp. 83-92.
10. A. J. Chamkha, A. M. Rashad, E. Al-Meshaiei, Melting effect on unsteady hydromagnetic flow of a nanofluid past a stretching sheet, Int. J. Chem. React. Eng, 9 (2011), pp. 1-13.
11. S. Ahmad, I. Pop, Melting Effect on Mixed Convection Boundary Layer Flow About a Vertical Surface Embedded in a Porous Medium: Opposing Flows Case, Transp. Porous Media., 102 (3) (2014), pp. 317-323, 10.1007/s11242-014-0291-x.
12. A. Ishak, R. Nazar, N. Bachok, I. Pop, Melting heat transfer in steady laminar flow over a moving surface, Heat Mass Transf., 46 (4) (2010), pp. 463-468.
13. T. Hayat, M. Mustafa, Z. Iqbal, A. Alsaedi, Stagnation-point flow of couple stress fluid with melting heat transfer, Appl. Math. Mech., 34 (2) (2013), pp. 167-176.
14. N. A. Yacob, A. Ishak, I. Pop, Melting heat transfer in boundary layer stagnation-point flow towards a stretching/shrinking sheet in a micropolar fluid, Comput. Fluids, 47 (1) (2011), pp. 16-21.
15. T. Hayat, M. Mustafa, S. Shehzad, S. Obaidat, Melting heat transfer in the stagnation-point flow of an upper-convected Maxwell (UCM) fluid past a stretching sheet, Int. J. Numer. Methods Fluids, 68 (2) (2012), pp. 233-243.
16. S. U. S. Choi, Enhancing thermal conductivity of fluids with nanoparticles, Am. Soc. Mech. Eng. Fluids Eng. Div. FED., 231 (1995), pp. 99-105.
17. M. Siavashi, M. Vahabzadeh Bozorg, M. H. Toosi, A numerical analysis of the effects of nanofluid and porous media utilization on the performance of parabolic trough solar collectors, Sustain. Energy Technol. Assessments., 45 (2021), p. 101179.
18. S. Mukhopadhyay, Effect of thermal radiation on unsteady mixed convection flow and heat transfer over a porous stretching surface in a porous medium, Int. J. Heat Mass Tran., 52 (2009), pp. 3261-3265.
19. A. Shahid, The effectiveness of mass transfer in the MHD Upper-Convected Maxwell fluid flow on a stretched porous sheet near stagnation point: a Numerical Investigation, Invension, 5 (4) (2020), pp. 64-79.

20. Zainal N. A., Nazar R., Naganthran K., Pop I., MHD flow and heat transfer of hybrid nanofluid over a permeable moving surface in the presence of thermal radiation, Int. J. Numer. Methods Heat Fluid Flow, 31 (3) (2020), pp. 858-879.
21. Khan S. A., Khan M. I., Hayat T., Alsaedi A., Darcy-Forchheimer hybrid (MoS2, SiO2) nanofluid flow with entropy generation, Comput. Methods Programs Biomed., 185 (2020), Article 105152.
22. Lund L. A., Omar Z., Dero S., Khan I., Baleanu D., Ni sar K. S., Magnetized flow of Cu2Al2O3+H2O hybrid nanofluid in porous medium: analysis of duality and stability, Symmetry, 12 (9) (2020), p. 1513.
23. Yusuf T. A., Mabood F., Khan W. A., Gbadeyan J. A., Irreversibility analysis of Cu-TiO2-H2O hybrid-nanofluid impinging on a 3-D stretching sheet in a porous medium with nonlinear radiation: Darcy-Forchhiemer's model, Alexand. Eng. J., 59 (2020), pp. 5247-5261.
24. A. Behseresht, A. Noghrehabadi, M. Ghala mbaz, Natural-convection heat and mass transfer from a vertical cone in porous media filled with nanofluids using the practical ranges of nanofluids thermo-physical properties, Chem Eng Res Des, 92 (3) (2014), pp. 447-452.
25. M. Ghalambaz, A. Noghrehabadi, A. Ghanb arzadeh, Natural convection of nanofluids over a convectively heated vertical plate embedded in a porous medium, Braz J Chem Eng, 31 (2) (2014), pp. 413-427, 10.1590/0104-6632.20140312s00001956.
26. S. Mehryan, M. Izadi, M. A. Sheremet, Analysis of conjugate natural convection within a porous square enclosure occupied with micropolar nanofluid using local thermal non-equilibrium model, J. Mol. Liq., 250 (2018), pp. 353-368.
27. T. Hayat, M. Imtiaz, A. Alsaedi, Melting heat transfer in the MHD flow of Cu–water nanofluid with viscous dissipation and Joule heating, Adv. Power Tech., 27 (2016), pp. 1301-1308.
28. S. Das, H. K. Mandal, R. N. Jana, O. D. Makinde, Magneto-nanofluid flow past an impulsively started porous flat plate in a rotating frame, J. Nanofluids, 4 (2015), pp. 167-175.
29. A. J. Chamkha, A. M. Aly, M. A. Mansour, Similarity solution for unsteady heat and mass transfer from a stretching surface embedded in a porous medium with suction/injection and chemical reaction effects, Chem. Eng. Commun., 197 (2010), pp. 846-858.
30. N. Sandeep, V. Sugunamma, Radiation and inclined magnetic field effects on unsteady hydromagnetic free convection flow past an impulsively moving vertical plate in a porous medium, J. Appl. Fluid Mech., 7 (2014), pp. 275-286.
31. P. Rana and R. Bhargava, Flow and heat transfer of a nanofluid over a nonlinearly stretching sheet: A numerical study, Commun. Nonlinear Sci. Numer. Simulat., 17 (2012) pp. 212-226.